Available online at www.sciencedirect.com
SCIENCE DIRECT
ELSEVIER
International Journal of Mass Spectrometry 252 (2006) 100–109
International Journal of Mass Spectrometry
www.elsevier.com/locate/ijms

Study of competing decay processes in small carbon clusters using time-resolved photoelectron imaging

F. Pagliarulo, B. Climen, B. Baguenard, F. Lépine, M.A. Lebeault, A. Ollagnier, J. Wills, C. Bordas *

Laboratoire de Spectrométrie Ionique et Moléculaire, UMR CNRS no. 5579, Bât. Kastler, Université Claude Bernard Lyon I, 43 Boulevard du 11 Novembre 1918, F69622 Villeurbanne Cedex, France

Received 13 January 2006; received in revised form 16 January 2006; accepted 17 January 2006
Available online 23 March 2006

Abstract

Atomic clusters may often be considered as small pieces of bulk material; however they may also exhibit properties radically different both from the atomic species and from the condensed phase. Photoemission is one of the many powerful methods to investigate clusters and size-effects in such systems, with very often non monotonous size-evolution. In atomic clusters, the finite-size equivalent of photoemission effects can be studied in details: both direct (photoionization or photodetachment, analogous to photoelectric effect) and delayed (analogous to thermionic emission) processes exhibit many features that may differ from the bulk behavior. Time-resolved photoelectron velocity-map imaging is used to analyze these processes in the case of small carbon anion clusters as well as in fullerenes.

PACS: 36.40.−c; 33.60.−q

Keywords: Photoemission; Photoelectron spectroscopy; Thermionic emission; Fragmentation

1. Introduction

In 1905, known as the *annus mirabilis*, Einstein proposed his interpretation of the photoelectric effect [1]. About a hundred years later, photoemission has become a routine method to investigate electronic properties of matter. The principle of photoelectron spectroscopy relies on the seminal Einstein equation $h\nu = \varepsilon + E_0$ which is a direct consequence of energy conservation. This equation states that if a system absorbs a photon of energy $h\nu$ larger than the electron binding energy E_0, it can be ionized and eject an electron of kinetic energy ε. In fact, more precisely, photoelectron spectroscopy relies on a general formulation of the Einstein equation where the binding energy E_0 is replaced by a binding energy E_i associated to a specific excited quantum state of the system (E_0 corresponding to the ground state). The kinetic energy ε of the emitted electron depends therefore on its binding energy E_i. Hence, the kinetic energy spectrum of these "direct" electrons provides a detailed quantum description of the system. However, photoexcitation processes are not always simple due to couplings between the various degrees of freedom of the system and part of the excitation energy may well be converted into internal energy. Indeed, at the beginning of the 20th century, the validity of the Einstein relationship was found to be correct, but not complete. In particular, it failed to account for the fact that the emitted electron energy and the photoelectric current are influenced by the temperature of the solid. For instance, the photoemission threshold was found at lower photon energy for a piece of hot metal. In these situations, interactions between degrees of freedom make a complete quantum description hardly possible. Better than Einstein description for direct electron emission, a statistical point of view has been developed to describe these indirect processes. The strength of the statistical framework comes from its ability to describe complex phenomena based on a few general concepts like density of states, temperature, entropy. For instance, emission of electrons from a hot metal is known as thermoelectric effect (or thermionic emission) and is very well described in terms of thermodynamic behavior.

Photoelectron spectroscopy experiments are currently performed on systems from simple atoms to bulk matter and very

* Corresponding author.
E-mail address: bordas@lasim.univ-lyonl.fr (C. Bordas).

1387-3806/$ – see front matter © 2006 Elsevier B.V. All rights reserved.
doi:10.1016/j.ijms.2006.01.053

different processes are observed. The connection between the results obtained for microscopic and macroscopic systems is far from being trivial. This is one of the reasons why atomic clusters have been extensively studied during the last decades [2]. Clusters are often considered of fundamental interest because they make the bridge between atomic microscopic and bulk macroscopic properties. This assessment is strikingly true when one studies indirect processes like delayed electronic emission. Clusters are model systems to investigate "cooling" processes, and understanding how a highly excited system can release its excess energy. Delayed electron emission is one of these cooling processes and statistical interpretation is very tempting since, from many respects, it resembles the very well known thermoelectronic effect in bulk matter.

Indirect processes are actually by far more important in clusters than in bulk matter. This is linked to the fact that in the case of clusters we are dealing with a finite heat-bath where the absorption of a single photon changes qualitatively the state of the system. In bulk matter the absorption of a photon by a piece of metal does not change significantly its internal state. The excess energy is either released by ejecting an electron, or dissipated in the bulk, without any electron emission, and the temperature of the metal remains the same. This is totally different for a small cluster. After the absorption of a photon, the excited cluster may release its energy very rapidly by emitting an electron. However, there is very often a substantial probability that the internal energy is shared among various degrees of freedom. The very strong couplings among the excited states lead very rapidly to a complete equilibrium and to a thermalization of the system on a femtosecond or picosecond timescale. The temperature of the cluster increases significantly by an amount on the order of $h\nu/C_v$, where C_v is the heat capacity of the cluster. The increase in temperature for a small system containing 10 atoms and absorbing a UV photon of 4 eV is typically about 2000 K. In the case of carbon cluster anions, 4 eV is largely above the electron binding energy for clusters with less than 20 atoms. Further, the decrease of the temperature after the ejection of the electron is also on the order of 1000 K for a 10 atoms cluster. This means that even though one starts with a cold system, the excited cluster may be considered as a very hot nanofilament and one has to take into account thermionic emission from the cluster that, in some cases, may exceed direct emission.

In the following, we will focus on thermionic emission although in some cases dissociation channels may be largely dominant, particularly in C_{60}. Indeed, owing to its very general occurrence delayed electron emission [3] has been the focus of numerous studies. Strictly speaking, and following the analogy with condensed matter physics, delayed electron emission from clusters is described as thermionic emission when the excitation energy is equally partitioned among the various electronic and nuclear degrees of freedom. Most early studies of thermionic emission in clusters were performed with standard ion time-of-flight techniques or measurement of the total photoelectron current as a function of time delay [4–6]. More detailed studies have subsequently been performed by measuring time-integrated photoelectron spectra [7–11]. Both methods suffer however from a lack of generality and it is clear that only a time-resolved measurement of the kinetic energy distribution of the ejected electrons as a function of the delay after excitation could provide a global understanding of thermionic emission in clusters. The intrinsic capability of charged particle imaging [12] to combine energy and time resolution has allowed developing a photoelectron spectrometer with time resolution well adapted to the timescale of delayed emission (nanosecond to microsecond) [13]. It is based on the elegant principle of velocity-map imaging [14]. Time resolved photoelectron spectroscopy is a very powerful tool that allows us to test thermodynamics or statistical description of finite-size systems.

In this article, we present two characteristic different examples of delayed emission processes in small clusters. First, studies of the photodetachment of small C_n^- clusters in the size range $n = 10$–22 [13,15] using time-resolved imaging will be presented. In that case, a single near-UV photon may induce direct photodetachment. One of the advantages of working with anions is that mass-selection is easily achievable, which is of course required for that kind of experiment. Another characteristic of small anions in single photon regime is that they are simple models of refractory systems in the sense that the electron binding energy is much lower than the dissociation or fragmentation energy; therefore the electronic emission is by far the dominant decay channel. For those systems, an explicit distinction between direct and delayed processes could be obtained that was not achieved in previous experiments [16]. The situation is radically different in the second example presented below, namely in the case of the fullerene C_{60}, that has often been used as a paradigm for thermionic emission [6,17–20]. In that case, the binding energy of the electron exceeds significantly the photon energy under our experimental conditions. Ionization of C_{60} requires a large amount of internal energy following multiphoton excitation and there is no direct emission processes. In that case, competition with numerous dissociation channels cannot be avoided, as well as the broad internal energy distribution consecutive to multiphoton ionization. Once again, time-resolved imaging [21,22] allows to separate unambiguously thermionic emission from other processes and to follow the time-evolution of the decay. Moreover, electron spectra can give insights on the dissociation channel. Before entering into the overview of the experimental results in these two examples, let us first describe briefly the unified theoretical framework adapted to the treatment of delayed emission processes in finite-size systems.

2. Theoretical background

Various theoretical approaches maybe followed to describe processes resulting from a statistical redistribution of internal energy [23]. One of the more general is the so-called detailed balance theory. This unified framework introduced in the early days of quantum mechanics by Weisskopf [24] is described in details in recent articles [22,25,26]. Under the assumption of thermal equilibrium and reversibility of quantum processes, the detailed balanced theory allows expressing the differential thermionic

emission rate as follows:

$$k_{el}(E,\varepsilon) = \frac{2m}{\pi^2\hbar^3}\sigma(\varepsilon)\varepsilon \exp\left(-\frac{\varepsilon}{k_B T_d}\right) \exp\left(-\frac{\Phi}{k_B T_e}\right) \quad (1)$$

where ε is the electron kinetic energy, m and $\sigma(\varepsilon)$ are respectively the electron mass, and the cross-section for electron capture, Φ is the electron binding energy (electron affinity for anions, ionization potential for neutrals). The microcanonical temperatures appearing in Eq. (1) are respectively the daughter temperature T_d (temperature of the system after emission) and the emission temperature T_e. These quantities depend explicitly on the internal energy E: T_d is the temperature of a system of internal energy $E_d = E - \Phi$ while T_e is the temperature of a system of internal energy $E_e = E - \Phi/2$. In the limit of the low kinetic energy regime and without lack of generality the differential rate maybe written as:

$$k_{el}(E,\varepsilon) = C(E)\varepsilon^{\gamma} \exp\left(-\frac{\varepsilon}{k_B T_d}\right) \quad (2)$$

where $C(E)$ is a factor that depends only on the total energy E and on intrinsic properties of the system. The exponent γ includes the kinetic energy dependence of the capture cross-section and depends explicitly on the nature of the interaction potential between the electron and the daughter fragment. Note that the kinetic energy profile of the photoelectron spectrum depends only on the final (daughter) temperature of the system.

Through standard approximations of the capture cross-section [27] and assuming spherical symmetry, the exponent appearing in Eq. (2) maybe specified: for finite-size neutral systems this exponent is $\gamma = 0$, while it is $\gamma = 1/2$ for anions. In the limit of bulk matter $\gamma = 1$, this is another difference between clusters and bulk matter. Note that Eq. (1) allows deriving similar formula for dissociation processes with different values of the exponent γ.

The microcanonical thermionic emission rate $K_{el}(E)$ is obtained by integrating Eq. (1) over the kinetic energy ε. It may be written in an Arrhenius form as follows:

$$k_{el}(E) = \omega(E) \exp\left(-\frac{\Phi}{k_B T_e}\right) \quad (3)$$

where the prefactor ω depends slowly on the energy E. If an initial internal energy distribution $g(E,t=0)$ is considered, kinetic energy spectrum is obtained by integrating Eq. (1) over E weighted by $g(E,t)$. A spectrum recorded in a finite time window will correspond to the superimposition of spectra of a distribution of subsystems having different energy E. A very important remark concerns the extremely rapid evolution of the rate $K_{el}(E)$ as a function of total energy E. That is to say, a small change in E induces a large change of the timescale of the process under consideration. This is in some sense a very convenient property since the electron kinetic energy spectrum recorded in our experiment at a given delay will correspond mainly to systems with a well-defined internal energy. This allows us to derive the following general expression for the time-dependent energy spectrum [22]:

$$P(\varepsilon,t) = A(t)\varepsilon^{\gamma} \exp\left(-\frac{\varepsilon}{k_B T_{eff}(t)}\right) \quad (4)$$

In brief, experimental photoelectron spectrum can be compared directly with a profile given by Eq. (2) with the adequate value of the γ exponent. Fit of the experimental data to this formula will allow deriving an explicit value of the daughter temperature T_d. On the other hand, integrated emission rate, connected to the emission temperature T_e via Eq. (3) allows a comparison between energy-dependent and time-dependent measurements owing to the close connection between T_d and T_e.

3. Experimental set-up

The experimental installations used to study time-resolved photodetachment of small carbon clusters or photoionization of C_{60} are rather similar and combine laser vaporization techniques for the production of free clusters and time-of-flight mass spectrometry and time-resolved photoelectron imaging for the detection. The main difference between both arrangements lies in the coupling between the molecular beam and the electron spectrometer. Small carbon anion clusters C_n^- [15] are produced by laser ablation of a graphite rod using a tightly focused laser beam (second harmonic of a Nd:YAG). Carbon clusters are formed in the supersonic expansion in a pulse of helium carrier-gas. Native anions are extracted using a pulsed electric field in the extraction region of a time-of-flight mass spectrometer (TOFMS). Clusters of specific mass, selected by their time-of-flight, are then excited by a second laser beam (Xe:Cl, 308 nm, pulse duration 15 ns, or Xe:Cl pumped dye laser) above their photodetachment threshold in the center of the interaction region of the photoelectron imaging spectrometer. The excitation of a well-defined cluster mass is ensured by firing the excitation laser when the given size is precisely at the center of the electron spectrometer. In the case of C_{60}, a beam of fullerenes is produced either by laser desorption of pure C_{60} embedded in a rod of organic material (matrix-assisted laser desorption), or by evaporation in a thermal oven. The first technique provides a very high flux with however a high velocity that prevents the observations at delays larger than a few microseconds. The oven technique is better for observations at delays in the range 2–20 μs since the velocity of fullerenes is reduced. However, the oven production is not appropriate to the study of photoions resulting from the fragmentation processes (not described in the present article) owing to the large velocity-drift that induces distortions of the images. As opposed to the case of anion clusters, no mass-selection is required and the C_{60} molecular beam enters directly the velocity-map imaging spectrometer where optical excitation is achieved using nanosecond tunable dye laser in the range 220–400 nm. In that case, the extraction region of the electron spectrometer is at the same time the extraction region of the TOFMS. The C_{60} set-up allows the measurement of mass spectra and of photoelectron spectra under strictly identical experimental conditions simply by adapting the electrode voltages to the desired purpose.

The last element in the experimental set-up, namely the velocity-map imaging spectrometer itself, is strictly identical in the case of anion or neutral systems. The principle of charged particle imaging introduced in the early 1980s [28] is extremely simple. A static electric field is applied in the interaction region and used to project the photoelectrons produced in photodetachment or photoionization onto a position sensitive detector (PSD). This PSD is made up of a tandem microchannel plates followed by a phosphor screen and a CCD camera for read-out. The electrodes of the spectrometer and the applied voltages are designed such that the resulting extraction field projects the electrons onto the PSD with a position of impact that depends only on the electron initial velocity, irrespective of its initial position in a volume of a few cubic millimeters around the center of the spectrometer. This is the principle of velocity-map imaging [14]. By summing electron impacts over many laser shots we obtain an image that is a map of the projection of the electrons velocity on a plane perpendicular to the electric field. If the laser polarization is fixed parallel to the detector, a standard inversion method [12,29] allows obtaining the distribution of velocity both in modulus and in direction, i.e., an angular-resolved photoelectron spectrum. Since the measurement of the electron velocity relies entirely on geometrical properties of the electron trajectories and since the time of flight of the electron is almost independent on its velocity (the kinetic energy acquired in the external field is by far much larger than the initial kinetic energy) velocity-map imaging presents the priceless advantage, with respect to standard photoelectron spectroscopy techniques like, e.g., magnetic-bottle [30], that it is intrinsically capable of time-resolution. Indeed, the time of impact of the electron onto the PSD is directly connected to the time of emission of the electron. Therefore, by simply gating the microchannel plates, one can select a given time slice in the electron distribution and then record a delayed emission spectrum in a well-defined time window after excitation. The time resolution of our system is, for the moment, limited to about 60 ns, which is appropriate to the timescale of the observed phenomenon. However, the same principle could allow a nanosecond resolution provided an improvement of the read-out electronic is achieved. In addition, the detection efficiency of velocity-map imaging is constant at threshold, which is particularly useful for measuring the slow photoelectron energy distributions corresponding to the emission of thermal electron from hot clusters. Time resolved velocity-map imaging was used for the first time in the case of thermionic emission of C_{60} [21], and further extended to the study of other systems. A review of this method has been published recently [13].

4. Thermionic emission in small carbon anion clusters

Small carbon anion clusters are prototypical systems to study thermionic emission free from other competing channels. Indeed, the electron binding energy in small C_n^- carbon clusters (the electron affinity) is included roughly between 2.0 and 3.6 eV (ring isomers) in the range $n = 10$–22, while the fragmentation energy is well above 5.0 eV [31]. This characteristic allows, first, to reach the detachment continuum by single photon excitation using standard laser systems. Second, following excitation in the near-UV at 4.0 eV, the photodetachment channel is open while all fragmentation channels are closed. Besides, even when taking into account a possible substantial internal energy prior to optical excitation, the thermionic emission rate exceeds largely the estimate of all other decay rates.

Fig. 1 presents typical experimental results obtained in the photodetachment of C_{18}^- at 308 nm (about 1.3 eV above the electron affinity) recorded at two different delays after excitation. The inverted image on the top left panel of Fig. 1 was recorded with the laser pulse synchronized with the centre of the detection time window in order to record full direct emission signal. This corresponds to the time gate where the major part

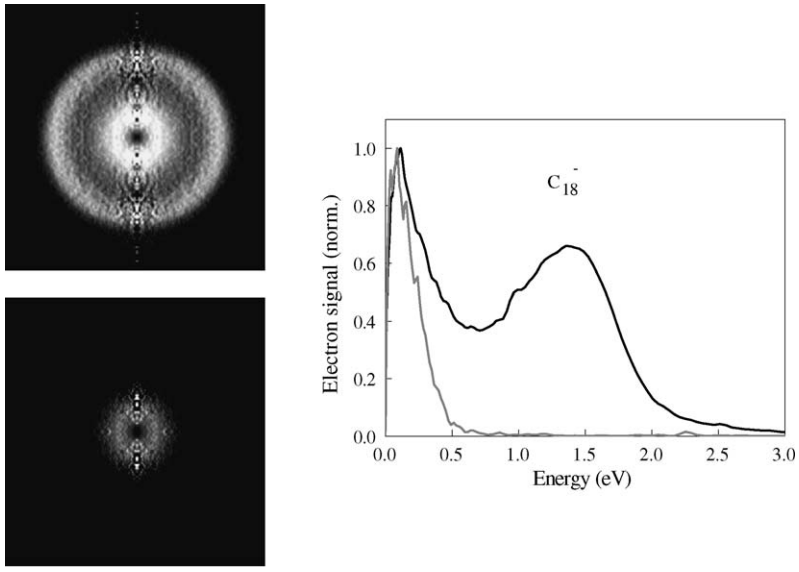

Fig. 1. Experimental results obtained in the photodetachment of C_{18}^- clusters at 308 nm. Top left: inverted synchronized image (−30 to +30 ns detection gate) including full direct emission and the early stage of delayed emission. Bottom left: delayed image (60–120 ns detection gate) where only delayed emission remains. Right—corresponding photoelectron spectra: direct (black line) and delayed (grey line) spectrum.

of electrons is ejected and it is rather similar to a time-integrated image [16]. The largest ring in the synchronized image corresponds to fast electrons, ejected with the largest amount of kinetic energy. This structure is slightly anisotropic (anisotropy is more pronounced at some sizes) as it can be seen in the figure, and its size increases when the photon energy is increased. Therefore, this structure maybe attributed to direct emission. On the contrary, the structure in the middle, at low energy, is almost independent on the excitation energy, and could correspond to delayed electron emission. The inverted image on the bottom left panel, was recorded after shifting the centre of the gate to 90 ns after the laser pulse (only electrons ejected 60–120 ns after the firing of the laser pulse are detected). This delay is long enough to remove completely direct emission, albeit short enough to keep a significant level of signal. The resulting images is significantly different: while two rings were clearly visible in the synchronized image (top), the external ring disappears completely in the delayed image (bottom) and only the inner structure remains. Note that the disappearance of the external ring confirms its initial attribution to direct photoemission, while the survival of the inner structure confirms that it corresponds to delayed emission even when detecting prompt electrons. Time-resolved imaging allows therefore a visible distinction between direct and delayed emission processes and there is no longer any ambiguity on the nature of the two processes.

The results obtained on carbon anions are summarized in Fig. 2 where a series of spectra with n ranging from 10 to 22 is presented. Black solid lines correspond to prompt electrons, grey solid lines to delayed electrons (same gate window as in Fig. 1). All spectra are normalized to same highest value in order to make comparison easier. Note however that the ratio between direct and delayed spectra differ significantly (intensity of the delayed spectrum being of course significantly lower than intensity of the direct one) from one size to the next, in connection with the evolution of the emission rate. In most cases, two principal features are visible in the synchronized spectra: one at low energy (below 0.5 eV) and another one at higher energy. The latter is assigned to direct emission based on the known values of the electron affinities of C_n^- clusters [11] and on the fact that this component rapidly vanishes as the time delay is increased. In the delayed spectra the high-energy feature has totally disappeared but the low energy feature remains. The remaining signal is due to electrons emitted over longer timescales through delayed emission. Delayed emission is identified without any ambiguity and a daughter temperature T_d of the clusters after decay may be estimated for each size through fits to Eq. (2) with the variable exponent $\gamma = 1/2$ relevant to the charge–dipole interaction between the electron and the remaining target in photodetachment. Delayed spectra are therefore fitted with the following formula where A and T_d are free parameters:

$$P(\varepsilon) = A\varepsilon^{1/2} \exp\left(-\frac{\varepsilon}{k_B T_d}\right) \quad (5)$$

Typical examples of such fittings are presented in Fig. 3. The excellent agreement visible for C_{20}^- for instance is typical of our observations above size 15. At smaller size the agreement is less satisfactory such as it is visible in the example of C_{14}^-. Even more significant discrepancies are observed on C_{10}^-

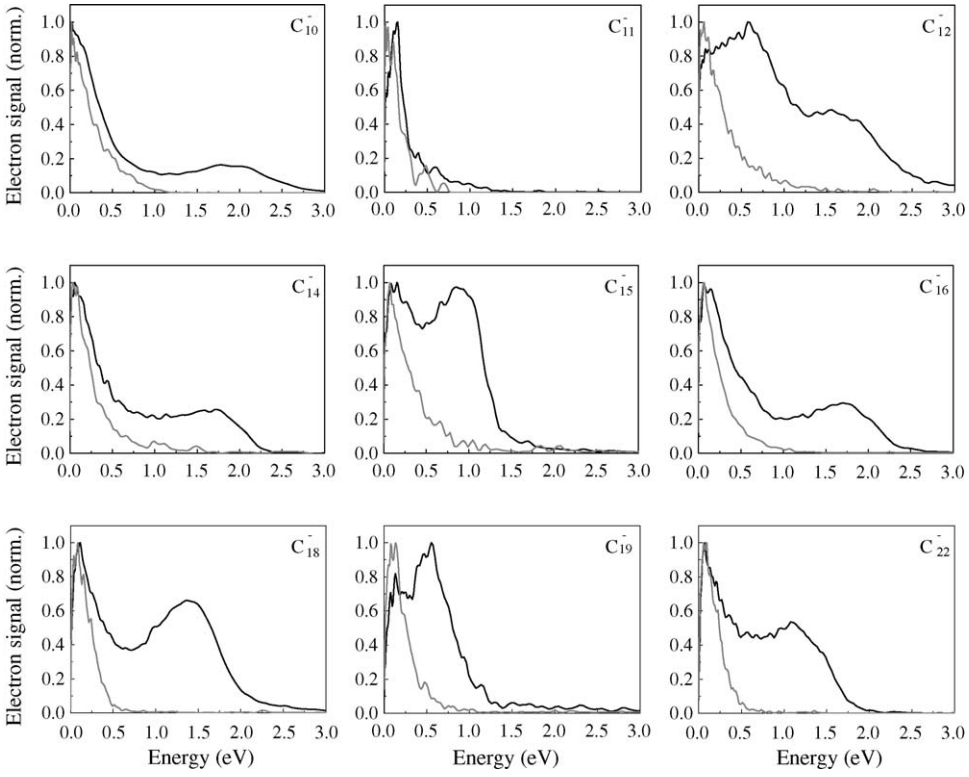

Fig. 2. Kinetic energy spectra of carbon cluster anions following excitation at λ = 308 nm for sizes n = 10–22. All spectra are normalized to same highest value and slightly smoothed. Black solid line: synchronized spectra (−30 to +30 ns detection gate). Grey solid line: delayed spectra (60–120 ns detection gate).

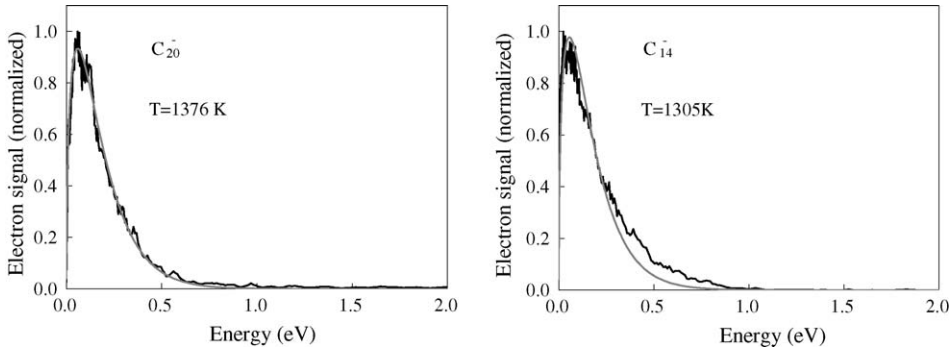

Fig. 3. Typical examples of fit of experimental delayed spectra (60 ns wide gate is open, 60 ns after the laser pulse, λ = 308 nm) with a kinetic energy profile as given by Eq. (5). At large size (example of C_{20}^- on the left) the agreement is excellent while at smaller size (example of C_{14}^- on the right) the comparison between experimental and model distribution is less convincing.

and C_{11}^- (see below). This aspect is discussed further at the end of the present section. Daughter temperatures derived from these fittings are displayed in Fig. 4 with error bars estimated based on fits to different experimental data. Fits are performed in the energy range (0–1 eV). Experimental temperatures are compared in Fig. 4 with various estimates of the expected temperature of the clusters. Two qualitatively different approaches have been followed. The first one is based on the assumption that clusters are thermalized to room temperature T_i before excitation, and that they absorb a single photon. It is therefore possible to evaluate the cluster daughter temperature following the absorption of a single photon of frequency ν from the heat capacity of the cluster C_v:

$$T_d = T_i + \frac{h\nu - \Phi}{C_v} \quad (6)$$

We actually use a more refined procedure to determine this temperature based on an estimation of the energy-dependent heat capacity $C_v(E)$ using the GAUSSIAN98 program package [32]. Multiphoton excitation can be neglected since we are working at low laser fluence. Further, no indication of multiple photon absorption could be noticed in the synchronized images. The daughter temperatures calculated according to Eq. (6) are compared with those derived from the fit for different cluster sizes in Fig. 4. Except at smaller sizes ($n = 10$, 11), the experimental value is by far larger than the calculated one. More specifically, for even clusters that have a low electron affinity the temperature calculated according to Eq. (6) is fairly large, while rather low temperatures are measured. On the contrary for odd clusters that have a higher electron affinity Eq. (6) leads to a smaller temperature, while in fact we measure a much larger temperature. Therefore, at least after a given delay of about 50–100 ns we can conclude from this noticeable discrepancy that the internal energy of the clusters that contribute to delayed emission after this delay is significantly different (in most cases larger) from the well-defined photon energy deposited in the cluster ($h\nu = 4.025$ eV). This strong discrepancy indicates most likely that the initial degree of internal excitation of the clusters is already significant; in particular this observation is not compatible with a cluster beam at room temperature. Without any explicit control of the initial cluster excitation, the assumption of control over cluster energies in the experiment is thus unfounded. In addition, comparing effective daughter temperatures with estimates of the temperatures based on a well-defined internal energy of the systems does not take into account the dynamics of the process and the essential relationship between the internal energy of the system and its typical decay time. In the framework of the detailed balance theory one can estimate the total emission rate as a function of the internal energy based on first principle arguments and on known values of the electron affinity [7,11]. Indeed, this rate varies extremely rapidly with the energy. In the range of interest, an increase of the emission temperature by only 50 K increases the emission rate (calculated according to detailed balance) by a factor of 2. As a consequence, it is obvious that only the clusters that have an internal energy such that the emission rate is roughly the inverse of the observation time window will contribute to thermionic emission. Those that have a larger internal energy will decay completely before the observation window; on the contrary those with smaller energy will wait longer before decaying.

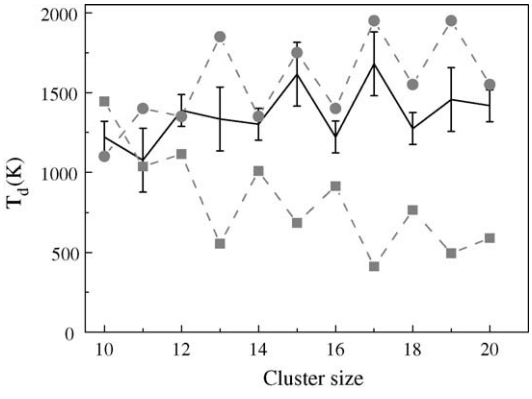

Fig. 4. Comparison of cluster temperatures derived from the experimental delayed spectra (black line with error bars) and calculated values. Grey squares: temperatures calculated assuming an internal energy given by the excitation photon energy $h\nu$. Grey circles: temperatures calculated based on the assumption of a thermionic emission rate of 10^7 Hz. Calculated values based on the assumption of rate-controlled thermionic emission are in much better agreement with experimental values.

Therefore, the second and more realistic approach used to analyze the experimental temperatures is based on the direct correspondence between the emission rate and the observation time window. This approach is evaluated in Fig. 4 through the

comparison of experimental and rate-determined temperatures, for a rate of 10^7 Hz (approximately the inverse of the observation delay). The variation of the emission rate as a function of temperature is estimated along the lines described in Section 2 and in Ref. [22]. Using this method for estimating the temperature the agreement between experimental results and predictions is much better. In particular the odd–even alternation is well reproduced. Clusters that have a higher electron affinity require more energy to emit an electron in a given time window and therefore the odd-parity clusters are found at higher temperature. With minor exceptions the general tendency is very well accounted for by this interpretation. This high degree of agreement between experimental results and a model based on the assumption of thermal equilibrium confirms the designation of delayed electron emission as thermionic emission. Note also that this direct correspondence between time – rate – and internal energy (or temperature) has been made possible thanks to time resolved photoelectron spectroscopy. The main conclusion of this part of the present work is that the characteristics of thermionic emission at a given time delay after excitation are entirely governed by the emission rate and a statistical description of the ongoing processes is well suited. The well-defined amount of energy deposited in the cluster has no direct influence on the observed phenomena. This aspect expresses also that the internal energy distribution of small anion clusters prior to photoexcitation is broad enough to support a final distribution including significant fraction of clusters having the proper degree of excitation to contribute in the given time range. In order to perform an experiment where the internal energy of the clusters would be precisely controlled by the excitation process, it is therefore necessary to develop a better control of the initial degree of thermalization excitation. This implies to work with cold clusters with initial temperatures below typically 100 K. This technical development is under progress in our laboratory in order to disentangle completely the effect of the initial excitation from the effect of the well-defined optical excitation.

Before concluding this section devoted to small carbon cluster anions let us finally discuss the discrepancies mentioned above regarding the adequacy of Eq. (5) for describing the profile of thermionic emission spectra in small systems. The discrepancies observed on C_{10}^- and C_{11}^- indicate most likely that the hard-sphere approximation of the capture cross-section has to be refined in those cases. Indeed, the geometry of these small systems is probably far from spherical symmetry; rather the linear isomer is expected to be dominant in our experiment. At larger sizes, the ring isomers dominate and, although not spherically symmetric, the model appears to be relevant for these species. Actually, a fit with Eq. (2) with a variable exponent γ allows to quantify the deviation from the spherical symmetry. This is shown in Fig. 5 where the delayed spectrum of C_{10}^- has been adjusted with a variable exponent. The effective value adapted to this small, probably linear, system is found to be $\gamma \approx 0.2$, which is significantly lower than the expected value of 1/2. In that case, the value of the fitted temperature is completely different but no conclusion should be drawn from this finding since the estimation of the temperature (see above) depends also on the detailed expression of the emission rate that depends explicitly on the

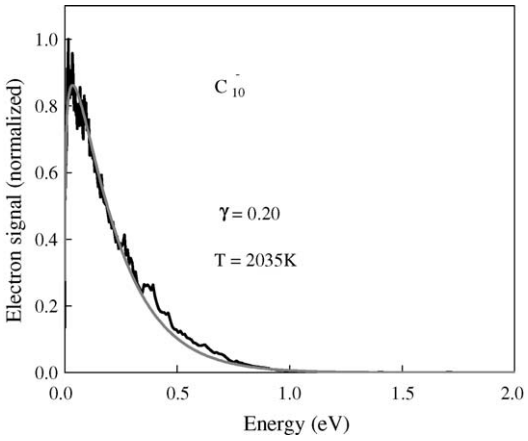

Fig. 5. Variable exponent adjustment according to Eq. (2) for delayed spectrum obtained in the photodetachment of C_{10}^-. Best agreement is found with $\gamma = 0.20$. More generally, at small sizes ($n = 10$–12) a much better agreement is found using a smaller variable exponent γ in the generalized formula. The low value of the exponent is probably linked to the non spherical symmetry of these small linear chains.

expression of the capture cross-section. Without going into the details, a much better agreement of experimental delayed electron emission with a general form given by Eq. (2) is found at small sizes ($n = 10$–13) using a smaller variable exponent γ in the range 0.2–0.3, while a value of 1/2 seems to be more appropriate to cluster sizes above $n = 14$. A classical model is being developed at the moment in order to evaluate the influence of the linear shape of the cluster on the electron capture cross-section that could explain these deviations. From now on however it appears reasonable to assume that the different emission profile observed in small C_n^- clusters is effectively linked to the geometry of these species. If confirmed, measurement of photoelectron spectra could be used as a probe of the capture cross-section itself.

5. Competition between thermionic emission and fragmentation in C_{60}

The second example selected to illustrate delayed emission processes in finite-size systems and the capabilities of time-resolved imaging is C_{60}. In fact this molecule is one of the favorite systems for studying delayed decay processes [6,17–20] owing first to the wealth of phenomena that it exhibits, and second owing to its ease of production. As far as the first aspect is concerned, the fullerene molecule C_{60} has been used to study various decay processes like delayed electron emission [6,17–20], blackbody radiation [33], sequential C_2 emission [34,35] and even multifragmentation [36]. At timescales relevant to our experimental conditions (laser pulse duration of about 10 ns and observation time window typically below 10 μs) multifragmentation and blackbody radiation may be neglected and the decay process in competition are essentially delayed ionization and C_2 emission.

This variety of phenomenon is not the only difference between fullerenes and carbon anion clusters. The ionization potential of C_{60} is much larger than the photon energy in the vis-

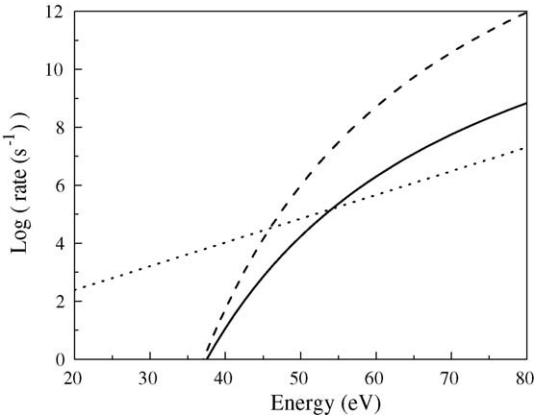

Fig. 6. Evolution of the decay rates as a function of the internal energy of C_{60}: thermionic emission rate calculated in the framework of the detailed balance theory (solid-line) [22]; C_2 emission rate estimated according to Ref. [22] (dashed-line). For comparison, the blackbody radiation rate which is defined as the number of photons emitted per second (dotted-line) [34] has been plotted. Typically for photon in the visible, its contribution is known to be negligible on the microsecond timescale.

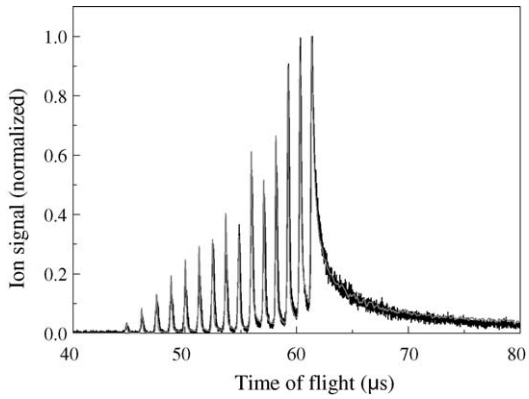

Fig. 7. Typical mass spectrum obtained in the photoionization of C_{60} (thin black solid line). The peak of C_{60}^+ exhibits a long tail towards large delays. This is the direct indication of delayed ionization. Smaller even-parity fragments resulting from the ejection of one or several C_2 fragments are clearly visible down to size $n = 32$. A Monte-Carlo simulation (broad grey solid line) is superimposed with the experimental data. Parameters used for estimating the various dissociation and thermionic emission rates are taken from Ref. [35].

ible or near-UV. Owing to the high values of the binding energy (ionization potential $\Phi \approx 7.6$ eV, C_2 binding energy $E_d \approx 11$ eV) and to the large number of degrees of freedom, the various emission rates become appreciable only for a substantial value of the internal energy. The variation of the thermionic emission rate and of the dissociation rate as a function of the internal energy of C_{60} maybe evaluated according to the detailed balance theory or to previous experimental results [34,35], respectively. Such an evaluation is presented in Fig. 6, together with the estimated blackbody emission rate. It is clearly visible in Fig. 6 that, in the region of interest for us (microsecond timescale), the decay of C_{60} occurs predominantly by emission of C_2 fragments. At lower internal energy, blackbody radiation cannot be ruled out and obviously plays a role at delays larger than about 10 μs although not directly visible. As a consequence the multiphoton excitation process is in a relatively high-order regime: typically more than 15 photons have to be absorbed by C_{60} to induce ionization over our typical timescales. Optical excitation using nanosecond laser does not prevent the system to absorb a substantial amount of internal energy and indeed, the examination of mass spectra with fragments as small as C_{32}^+ resulting unambiguously from sequential C_2 emission demonstrates that C_{60} molecules can absorb up to 100–150 eV under our experimental conditions. With respect to similar experiments using ultrashort laser pulses excitation [37] note also that the duration of the excitation process itself (about 10 ns) allows naturally for an internal energy redistribution after the absorption of every single photon. This leads to an almost perfect thermalization of the excited fullerenes. The assumption of statistical equilibrium is hence fully justified.

A typical time-of-flight (TOF) spectrum obtained in photoionization of C_{60} is presented in Fig. 7. The peak of C_{60}^+ ions is noticeably broadened and the long tail extending several tens of microsecond after the maximum is the clear indication of delayed ionization. Note that this tail does not present an exponential profile. Since it results from the sum over delayed ionization corresponding to a broad distribution of internal energy, the resulting signal is a power law t^{-p} where the characteristic exponent p is directly connected to the ratio of the binding energy of the two competing processes [6]. At shorter time-of-flights, all fragments peaks corresponding to successive loss of C_2 fragments, C_{58}^+, C_{56}^+... down to C_{32}^+ are also clearly visible in the mass spectrum. In Fig. 7, the experimental TOF spectrum is compared with a Monte-Carlo simulation of the chain of competing ionization and fragmentation processes schematized above. Similar simulations have already been published [35,38] based on more or less refined estimates of the decay rates relevant to all ionization or dissociation channels. This simulation is also based on the assumption of a given distribution of internal energy. Indeed, the appearance of the TOF spectrum is extremely sensitive to this distribution. This, in turn, allows to derive rather precisely the degree of excitation of the fullerenes. For a given laser intensity, the corresponding internal energy distribution following multiphoton excitation is given by a standard Poisson distribution. The total internal energy distribution at time $t = 0$: $g(E,0)$ results from a spatial averaging over regions with laser intensities varying from zero to the maximum value (the laser beam is narrower than the molecular beam). Below a cut-off energy $E_c = \bar{N}h\nu$ (average internal energy at the waist, the width of the Poisson distribution is roughly $\Delta E \approx \sqrt{\bar{N}}h\nu$), the absorbed energy follows a power law $g(E,t=0) \propto E^{-n}$ that has been estimated by other authors [35,38]. In accordance with previous results, the best agreement is obtained for $n = 2.5$. Above the cut-off energy, the distribution is simply Poisson-like. The agreement between the experimental TOF spectrum and the Monte-Carlo simulation is excellent as can be seen in Fig. 7. Despite the many unknowns regarding the various parameters entering the simulation (ionization potentials and dissociation energies of all neutral and cation fragments are known within significant uncertainties in some cases, rate prefactors are often poorly known) the quality of the agreement ensures a rather reliable derivation of the internal energy distribution, which, in

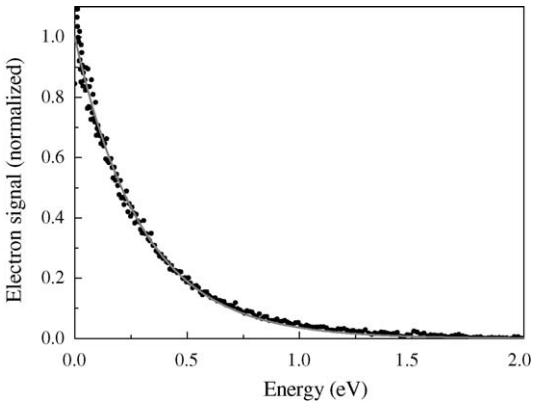

Fig. 8. Typical experimental spectrum (dots) recorded in the time range (200–300 ns) after excitation at $\lambda = 330$ nm (dots). Only thermionic emission from C_{60} is detected. An effective temperature of 3490 ± 100 K is fitted (solid line) to the experimental distribution.

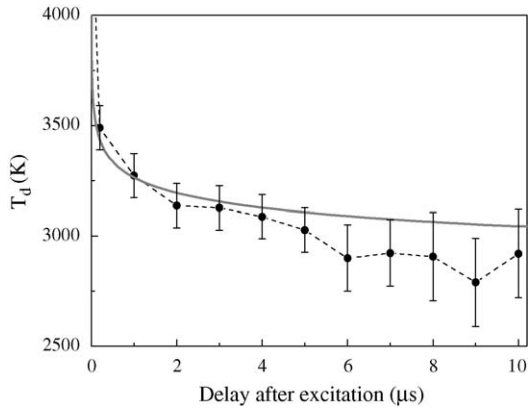

Fig. 9. Experimental daughter temperatures (black circle with error bars) extracted from fit to experimental spectra. Error bars increase with the delay due to the decrease of the electron signal. Integration time of 1 μs (except the point at short delay recorded with a 100 ns wide gate). Solid grey line is an estimate of the temperature based on our model which includes dissociation and thermionic emission channels [22]. The agreement is very satisfactory.

turns, allows a more refined interpretation of photoelectron spectra. Photoelectron images have been recorded with excitation in the range 220–400 nm, at laser fluences below 10^9 W/cm^2 (pulse duration 10 ns, 5–50 mJ/pulse). No significant dependence on the laser photon energy could be noticed. From the point of view of photoelectron spectra, the large width of the internal energy distribution following multiphoton excitation in the visible or near-UV implies that these various experimental conditions do not lead to significant differences in the internal energy distribution of the molecules and the photoelectron spectra do not differ significantly as a function of the laser intensity or wavelength. Indeed, photoelectron energy distribution is much less sensitive to the experimental conditions (except for the delay) than the fragmentation pattern observed in TOF spectra. Photoelectron images have been recorded with gate of width ranging from 100 ns to 1 μs and with delays ranging from 0 to 20 μs. At larger delays, photoelectron images were always recorded using the thermal oven source in order to minimize the beam velocity and to maximize the residence time in the effective detection region. However, owing to our experimental design, images recorded with a delay larger than about 10 μs are slightly distorted due to the drift velocity in the beam and no significant data could be derived at delays larger than 10 μs. From this point of view the laser desorption source is even worse since the velocity of the molecules in the beam is much larger (helium carrier-gas) but in that case the dispersion of velocity around the average value is significantly smaller and it turns out that the laser desorption method is more efficient and allows a better image resolution for photoions (results obtained with photoions will be discussed in a forthcoming paper). The typical experimental spectrum presented in Fig. 8 as well as the overview of daughter temperatures presented in Fig. 9 have been obtained at a laser wavelength $\lambda = 330$ nm under moderate intensity. Fig. 8 presents a time-resolved photoelectron spectrum resulting from the inversion of an electron image recorded using a 100 ns-wide gate, at a time delay of 200 ns after optical excitation. A least-square fit of the spectrum to Eq. (2) (solid line) with an exponent $\gamma = 0$ (relevant to ionization of a neutral species) leads to an effective daughter temperature $T_d \approx 3490 \pm 100$ K. Note the excellent agreement between experimental and calculated spectra. This excellent agreement confirms the validity of the detailed balance and of the dependence of the kinetic energy profile (through the γ exponent). The evolution of the daughter temperature extracted from a fit to the experimental spectra is presented in Fig. 9. In this figure, we present results averaged over different series of measurements using an integration gate of 1 μs over the range 0–10 μs (except for the point at 200 ns obtained with a narrower gate). Experimental errors in the range 100–200 K are estimated based on the dispersion of various data sets. The broad solid line is the result of a calculation based on the detailed balance assuming an internal energy distribution compatible with the one used to fit TOF spectra and standard parameters [22]. Except at larger delays where the measured temperature is systematically below the estimated one (although within the error bars), the agreement between our experimental results and estimates of the temperature based on parameters compatible with previous works [39] is a strong support of the validity of the detailed balance theory. From this point of view, the variation of the effective temperature as a function of time delay is a direct measurement of the evolution of the total decay rate (essentially the dissociation decay rate) as a function of temperature, which puts severe constraints on the couple of Arrhenius parameters (E_{diss}, ω_{diss}), respectively, dissociation energy and prefactor. This will be discussed in details in a separate article. Finally, the same conclusion than for carbon cluster anions holds for C_{60} fullerenes, namely, the effective temperature of the systems depends essentially on the time delay at which decay occurs, in other words there is a strong and direct connection between temperature and time of observation. At the same time, the relevance of the statistical approach is again justified.

Experimental images have also been recorded on photoions. These results will be published elsewhere. Let us however mention that the kinetic energy release measurements of the various ion fragments are another confirmation of the results obtained in TOF spectra or in photoelectron imaging.

6. Conclusion

The results relative to small carbon anion clusters or neutral fullerenes presented in this article allows to demonstrate the power of time-dependent photoelectron imaging that leads to an unambiguous discrimination between fast and delayed processes. Time-resolved velocity-map imaging is an invaluable tool to study electron emission processes on typical (rather long) timescales in the range from a few tens of nanoseconds to tens of microseconds.

From a more fundamental point of view, this clear distinction between the various ongoing processes combined with the description of thermionic emission and fragmentation processes in the framework of the detailed balance theory, has allowed us to verify simple laws for photoelectron kinetic energy distributions in the case of photodetachment and in the case of photoionization. This excellent detailed agreement between experimental results and model is also a strong confirmation of the validity of the detailed balance description that offers a unified understanding of the decay processes. The second fundamental conclusion, which is however not a new finding, is that there is a specific connection between time delay and temperature which implies that delayed processes are entirely controlled by the decay rates rather than by the amount of internal energy deposited in the systems, which in many cases is either not controlled or not sufficient to control the degree of internal excitation. On the other hand, a number of points remain to be elucidated among which the understanding of the detailed mechanisms of thermalization and the behavior at larger delays where blackbody radiation starts to play a role. In addition, it has been shown for smaller cluster sizes in the case of carbon cluster anions that the geometry of the system may play a role and induce a number of deviations from the simple threshold laws presented above. Classical calculations are in progress in order to interpret quantitatively these deviations assuming linear chain geometries.

Acknowledgments

The "Laboratoire de Spectrométrie Ionique et Moléculaire" is a "Unité Mixte de Recherche CNRS-Université Lyon 1" (UMR CNRS 5579). We acknowledge the support of the European Commission in the framework of the European Cluster Cooling Network (Contract No.: HPRN-CT-2000-00026).

References

[1] A. Einstein, Ann. Phys. (Leipzig) 17 (1905) 132.
[2] B. von Issendorff, O. Cheshnovsky, Annu. Rev. Phys. Chem. 56 (2005) 549.
[3] E.E.B. Campbell, R.D. Levine, Annu. Rev. Phys. Chem. 51 (2000) 65.
[4] B.A. Collings, A.H. Amrein, D.M. Rayner, P.A. Hackett, J. Chem. Phys. 99 (1993) 4174.
[5] S.E. Kooi, A.W. Castleman Jr., J. Chem. Phys. 108 (1998) 8864.
[6] K. Hansen, O. Echt, Phys. Rev. Lett. 78 (1997) 2337.
[7] S. Yang, K.J. Taylor, M.J. Craycraft, J. Conceicao, C.L. Pettiette, O. Cheshnovsky, R.E. Smalley, Chem. Phys. Lett. 144 (1988) 431.
[8] D. Ding, R.N. Compton, R.E. Haufler, C.E. Klots, J. Phys. Chem. 97 (1993) 2500.
[9] H. Handschuh, G. Ganteför, B. Kessler, P.S. Bechthold, W. Eberhardt, Phys. Rev. Lett. 74 (1995) 1095.
[10] G. Ganteför, W. Eberhardt, H. Weidele, D. Kreisle, E. Recknagel, Phys. Rev. Lett. 77 (1996) 4524.
[11] M. Kohno, S. Suzuki, H. Shiromaru, T. Moriwaki, Y. Achiba, Chem. Phys. Lett. 282 (1998) 330.
[12] B.J. Whitaker, Imaging in Molecular Dynamics, Cambridge University Press, 2003.
[13] B. Baguenard, J.B. Wills, F. Pagliarulo, F. Lépine, B. Climen, M. Barbaire, C. Clavier, M.A. Lebeault, C. Bordas, Rev. Sci. Instrum. 75 (2004) 324.
[14] A.T.J.B. Eppink, D.H. Parker, Rev. Sci. Instrum. 68 (1997) 3477.
[15] J.B. Wills, F. Pagliarulo, B. Baguenard, F. Lépine, C. Bordas, Chem. Phys. Lett. 390 (2004) 145.
[16] B. Baguenard, J.C. Pinaré, F. Lépine, C. Bordas, M. Broyer, Chem. Phys. Lett. 352 (2002) 147.
[17] E.E.B. Campbell, G. Ulmer, I.V. Hertel, Phys. Rev. Lett. 67 (1991) 1986.
[18] P. Sandler, C. Lifshitz, C.E. Klots, Chem. Phys. Lett. 200 (1992) 445.
[19] Y. Zhang, M. Stuke, Phys. Rev. Lett. 70 (1993) 3231.
[20] D. Ding, J. Huang, R.N. Compton, C.E. Klots, R.E. Haufler, Phys. Rev. Lett. 73 (1994) 1084.
[21] F. Lépine, B. Climen, F. Pagliarulo, B. Baguenard, M.-A. Lebeault, C. Bordas, M. Hedén, Eur. Phys. J. D 24 (2003) 393.
[22] F. Lépine, C. Bordas, Phys. Rev. A 69 (2004) 053201.
[23] W. Forst, Unimolecular Reactions, a Concise Introduction, Cambridge University Press, 2003.
[24] V. Weisskopf, Phys. Rev. 52 (1937) 295.
[25] J.U. Andersen, C. Gottrup, K. Hansen, P. Hvelplund, M.O. Larsson, Eur. Phys. J. D 17 (2001) 189.
[26] J.U. Andersen, E. Bonderup, K. Hansen, J. Phys. B 35 (2002) R1.
[27] C.E. Klots, J. Chem. Phys. 100 (1994) 1035.
[28] D.W. Chandler, P.L. Houston, J. Chem. Phys. 87 (1987) 1445.
[29] C. Bordas, F. Paulig, H. Helm, D.L. Huestis, Rev. Sci. Instrum. 67 (1996) 2257.
[30] P. Kruit, F.H. Read, J. Phys. E 16 (1983) 313.
[31] F. Lépine, A.R. Allouche, B. Baguenard, C. Bordas, M. Aubert-Frécon, J. Phys. Chem. A 106 (2002) 7177.
[32] M.J. Frisch, G.W. Trucks, H.B. Schlegel, G.E. Scuseria, M.A. Robb, J.R. Cheeseman, V.G. Zakrzewski, J.A. Montgomery Jr., R.E. Stratmann, J.C. Burant, S. Dapprich, J.M. Millam, A.D. Daniels, K.N. Kudin, M.C. Strain, O. Farkas, J. Tomasi, V. Barone, M. Cossi, R. Cammi, B. Mennucci, C. Pomelli, C. Adamo, S. Clifford, J. Ochterski, G.A. Petersson, P.Y. Ayala, Q. Cui, K. Morokuma, D.K. Malick, A.D. Rabuck, K. Raghavachari, J.B. Foresman, J. Cioslowski, J.V. Ortiz, B.B. Stefanov, G. Liu, A. Liashenko, P. Piskorz, I. Komaromi, R. Gomperts, R.L. Martin, D.J. Fox, T. Keith, M.A. Al-Laham, C.Y. Peng, A. Nanayakkara, C. Gonzalez, M. Challacombe, P.M.W. Gill, B. Johnson, W. Chen, M.W. Wong, J.L. Andres, C. Gonzalez, M. Head-Gordon, E.S. Replogle, J.A. Pople, Gaussian 98, Revision A.7, Gaussian Inc., Pittsburgh, PA, 1998.
[33] J.U. Andersen, C. Brink, P. Hvelplund, M.O. Larsson, B.B. Nielsen, H. Shen, Phys. Rev. Lett. 77 (1996) 3991–3994.
[34] C. Lifshitz, Int. J. Mass. Spectrom. 198 (2000) 1.
[35] B. Concina, S. Tomita, J.U. Andersen, P. Hvelplund, Eur. Phys. J. D 34 (2005) 191.
[36] S. Martin, L. Chen, R. Brédy, J. Bernard, M.C. Buchet-Poulizac, A. Allouche, J. Désesquelles, Phys. Rev. A 66 (2002) 063201.
[37] E.E.B. Campbell, K. Hansen, K. Hoffmann, G. Korn, M. Tchaplyguine, M. Wittmann, I.V. Hertel, Phys. Rev. Lett. 84 (2000) 2128–2131.
[38] K. Mehlig, K. Hansen, M. Hedén, A. Lassesson, A.V. Bulgakov, E.E.B. Campbell, J. Chem. Phys. 120 (2004) 4281.
[39] S. Tomita, J.U. Andersen, K. Hansen, P. Hvelplund, Chem. Phys. Lett. 382 (2003) 120.